J. Fluid Mech. (1993), *vol.* 254, *pp.* 1–21

The structure of the near wake of a sphere moving horizontally in a stratified fluid

By J. M. CHOMAZ[1,2], P. BONNETON[1] AND E. J. HOPFINGER[3]

[1] Meteo-France CNRM Toulouse, 42 avenue Coriolis, 31057 Toulouse, France

[2] LADHYX, Ecole Polytechnique, 91128 Palaiseau-Cedex, France

[3] LEGI-IMG, BP 53, 38041 Grenoble-Cedex, France

(Received 9 July 1992 and in revised form 30 November 1992)

We present experimental results for the wake structure of spheres moving in homogeneous and stratified fluid. In homogeneous fluid, the results of Kim & Durbin (1988) are confirmed and it is shown that the two characteristic frequencies of the wake correspond to two instability modes, the Kelvin–Helmholtz instability and a spiral instability. For the stratified wake four general regimes have been identified, depending principally on the Froude number F. For $F > 4.5$ the near wake is similar to the homogeneous case, and for $F < 0.8$ it corresponds to a triple-layer flow with two lee waves, of amplitude linear in F, surrounding a layer dominated by quasi-two-dimensional motion. Froude numbers close to one ($F \in]0.8, 1.5[$) give rise to a saturated lee wave of amplitude equal to half the sphere radius, which suppresses the separation region or splits it into two. Between $F = 1.5$ and 4.5 a more complex regime exists where the wake recovers progressively its behaviour in homogeneous fluid: the axisymmetry of the recirculating zone, the Kelvin–Helmholtz instability and, finally, the spiral instability.

1. Introduction

It is well known that stratification can strongly affect flow separation and the wake structure downstream of bluff bodies. Such flow configurations are encountered in the atmosphere, in the lee of hills or mountains and behind ridges in the oceans, and for this reason a considerable number of papers deals with lee waves and related flow problems. The two-dimensional flow of linearly stratified fluid past a circular cylinder or ridges has been most widely studied, both theoretically (Queney 1948; Long 1955; Miles & Huppert 1968) and experimentally (Davis 1969; Boyer *et al.* 1989). Flows past bodies of revolution are more complicated because stratification breaks the axisymmetry and a fluid parcel can move around or over the obstacle. The maximum height to which a fluid parcel is lifted can be estimated from energy considerations. In meteorology this is an important quantity to know in the context of cloud formation behind mountains. Equally important is a knowledge of the energy radiated by internal waves in the lee of the hill. Hunt & Snyder (1980) studied the stratified flow past surface-mounted obstacles, showing the suppression of flow separation at a Froude number of about 1. The collapse of the wake of bodies of revolution was investigated by Lin & Pao (1979), but the relation with the internal wave field was not considered. The most complete study in this respect is the numerical study by Hanazaki (1988) of the stratified flow past a sphere. This study was however limited to low Reynolds number ($Re = 200$).

In this paper we present results for the neutral and stratified wake of a sphere at moderate and large Reynolds numbers, $Re \in [150, 50000]$. Emphasis is placed on the interaction between the near-field turbulent wake and lee waves in stratified fluid for Froude numbers $F = U/NR \in [0.25, 12.7]$, where U and R are, respectively, the velocity and the radius of the sphere, and N the Brunt–Väisälä frequency. The structure of the wake in homogeneous fluid is presented as a necessary reference case.

The results presented here seem at first sight similar to those of Lin *et al.* (1992), published while the present paper was submitted. Although there is some desirable and clarifying overlap between the two papers, the results presented here are complementary in that the wake structure at large Froude numbers is treated in detail, whereas in the paper by Lin *et al.* this aspect is at most rather sketchy. The differences and similarities between the two papers will be discussed in §4.

2. Experimental methods

2.1. *Experimental apparatus*

Experiments were conducted in two different water towing tanks of respective sizes $0.5 \times 0.5 \times 4$ m^3 and $1 \times 3 \times 20$ m^3. The very large size of the latter is useful when long observation times are necessary, or when we want to avoid boundary (confinement) effects. This large size is also essential when the far-field wake is of interest. The stratification (NaCl solution) is obtained by a computer-monitored filling process which takes 8 hours for the large tank and 2 hours for the small one. In the present paper only linear stratification was considered with constant $N \in [0.67, 2.02$ rad/s], where $N = (-g/\rho_0 \, \mathrm{d}\rho/\mathrm{d}z)^{\frac{1}{2}}$.

Different techniques for supporting the sphere were tested, such as a continuous horizontal cable and a rod or profiled support, but all these perturb more or less seriously the flow close to the sphere. Finally, we adopted the three-wire configuration (see figure 1). The sphere was ballasted with lead grains and suspended by three stainless steel wires, of 0.1 mm in diameter. Reynolds numbers associated with these wires ranged from 0.8 to 40 and therefore no vortex shedding from them occurred and the total perturbation remained small enough to be neglected. Four spheres of radii $R = \{1.12, 2.5, 3.6, 5.0$ cm$\}$ were used in the experiments. Careful image analysis showed that, in the velocity range studied ($U \in [1, 50$ cm/s]), no vibration or oscillation were detectable. Probe measurements indicated slight vibrations in the velocity range $U < 10$ cm/s, however, which caused some problems in the detection of the spiral mode which is weak at low Re.

When, for a given stratification and a given sphere, the velocity is varied, the two dimensionless numbers $F = U/NR$ and $Re = 2RU/\nu$, where ν is the kinematic viscosity, evolve proportionally for each data set, in the form $Re(F) = Re(1)\,F$, where $Re(1) = 2R^2N/\nu$ is the Reynolds number for $F = 1$. The Froude and Reynolds numbers covered are $F \in [0.25, 12.7]$ and $Re \in [150, 50000]$. The ratio of sphere radius to half-depth of the channel (R/D) is small in the present experiments, ranging from $R/D = 0.022$ to 0.10. Confinement effects of the flow structure are likely to be negligible in the near field when $F_D = FR/D < 1/2\pi$ or $D > \lambda$, where D is the half-depth of the fluid layer and λ the wavelength of the lee wave.

2.2. *Visualization techniques*

Three techniques have been used in each sequence of experiments: a classical shadowgraph technique, particle streak photographs and laser-induced fluorescence. In the shadowgraph technique, images were formed on a frosted screen by means of

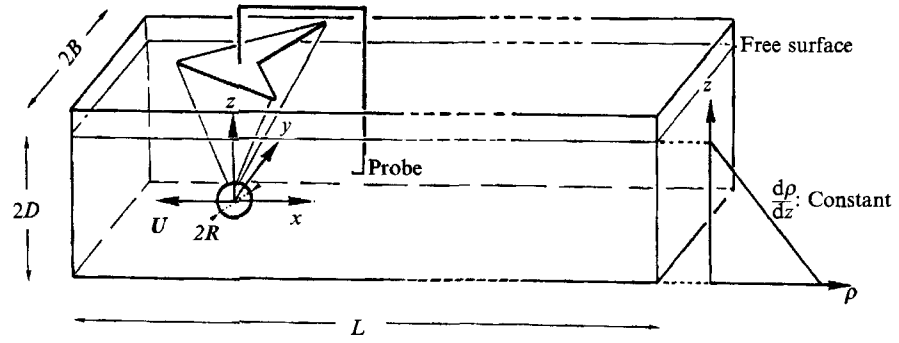

FIGURE 1. Experimental apparatus and definition sketch.

a nearly parallel commercial projector light traversing the fluid. For the particle streak photographs, neutrally buoyant particles of mean density 1.08 and of diameter between 0.1 and 0.3 mm, illuminated by a laser light sheet, were used. The very slow sedimentation of the particles in the stratified fluid (2 cm/day) allowed a uniform seeding of the fluid. Pictures of fluorescence induced by the laser were generated by depositing the dye either directly on the whole sphere surface or only on the front or rear part. The light source was a 5 W Argon laser and the light sheet was obtained by reflection of the laser beam on a vibrating mirror. The laser beam and the camera were fixed, or moving with the sphere, depending on which reference frame was of interest.

Images obtained by any of these techniques were recorded on a super VHS video recorder, using a black-and-white high-resolution CCD camera. Images were treated on-line or from the VCR by an image processing PC (board), allowing many standard manipulations. For images produced in this way, the treatment applied, if any, is specified in each figure caption.

2.3. *Measurement techniques*

Probe measurements were carried out in the big tank only, because long time series are necessary to detect characteristic frequencies of the wake. A quartz-coated hot-film velocity probe was pulled behind the sphere, at $x = 2R$ and $z = R$ above its centre (see figure 1). Furthermore, a conductivity probe was mounted flush with the surface of the sphere at 90° from the stagnation point on the top of the sphere. This probe consists of a platinum wire, 1.2 mm long and 25 μm in diameter, covered with platinum black. It was isolated from the metallic sphere, which plays the role of the second electrode, by an epoxy resin. This device can detect the density fluctuations due to the boundary-layer movements.

3. Experimental results

3.1. *Wake structure in homogeneous fluid* ($(F = \infty)$

In order to understand stratification effects on the wake of a sphere, a good knowledge of the wake in a homogeneous fluid is necessary. Unfortunately, existing results are somewhat controversial. Achenbach (1974) concluded that a change in the nature of the wake instability occurs at $Re = 6000$, whereas Kim & Durbin (1988) observed a two-frequency regime for all values of $Re > 800$ with no change at $Re = 6000$; the

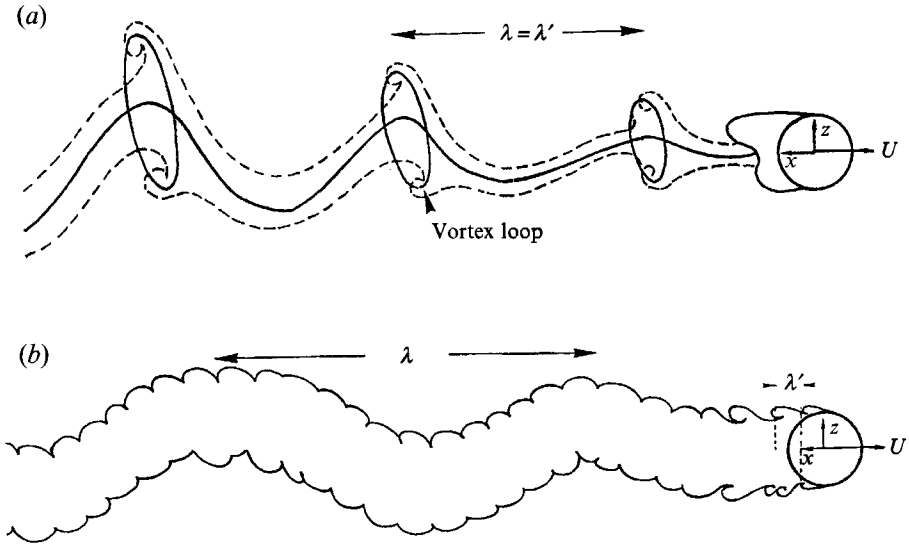

FIGURE 2. Schematic representation of the wake. λ', shearing mode wavelength; λ, spiralling mode wavelength. (*a*) $Re < 800$; (*b*) $Re > 800$.

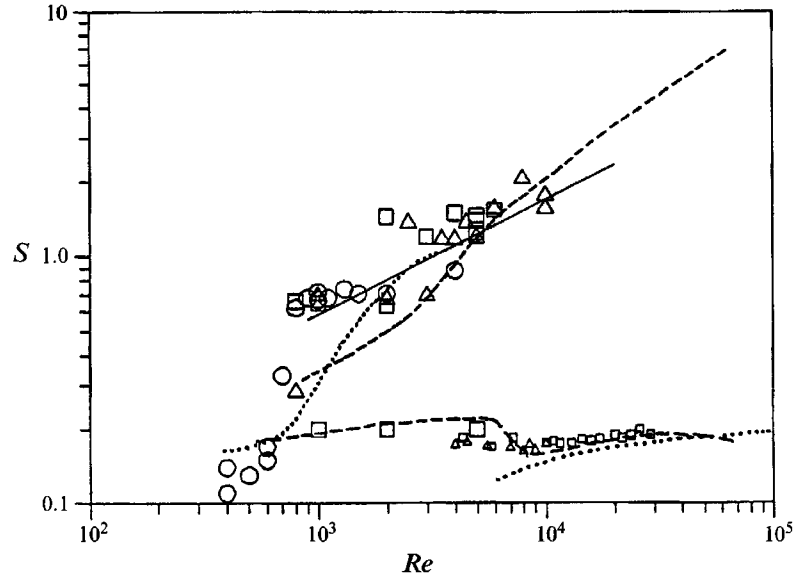

FIGURE 3. Strouhal number as a function of *Re*. ....., Achenbach (1974); ------, Kim & Durbin (1988); ——, S'_λ. Small symbols correspond to velocity probe measurements and large symbols to values determined from visualizations. ○, $R = 1.12$ cm; □, $R = 2.5$ cm; △, $R = 3.6$ cm.

higher frequency extends beyond $Re = 6000$ and the lower frequency is already present at $Re = 800$. Neither Achenbach nor Kim & Durbin fully succeeded in identifying the basic instability processes responsible for the two frequencies. They suggest that the high frequency is due to a Kelvin–Helmholtz instability, incoherent in the azimuthal direction and that the low frequency corresponds to a coherent rotation of the separation line on the sphere resulting in a spiral mode. The observations by Bonneton & Chomaz (1992), conducted at a time when we were not aware of the work of Kim

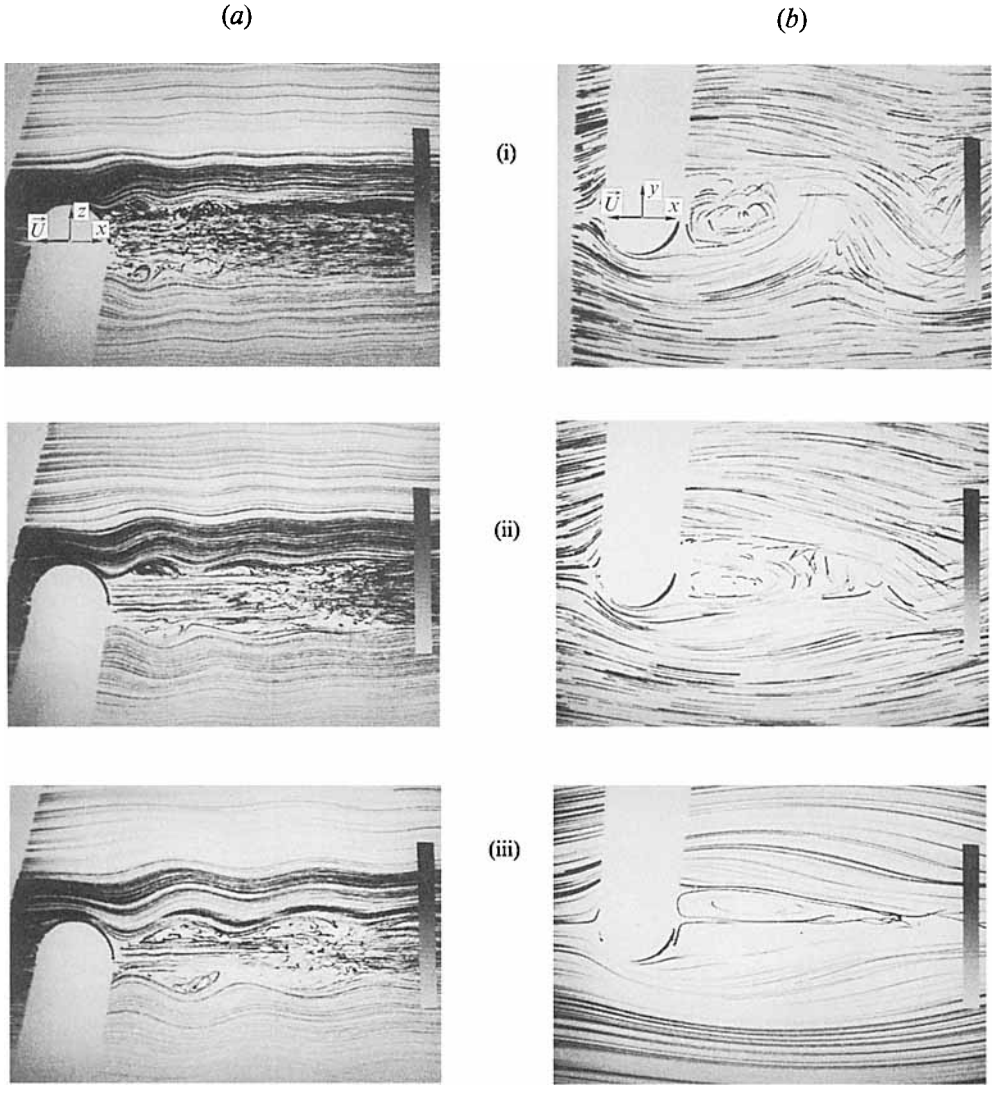

FIGURE 4 (i–iii). For caption see p. 7.

& Durbin, confirm the results of Kim & Durbin and clarify further the instability process. At $Re = 800$, two frequencies bifurcate continuously from a single-frequency state. The combination of flow visualizations and local probe measurements enabled us to link the spatial wake structure to the temporal behaviour revealed by the probe signals. In the Reynolds numbers range studied in homogeneous fluid, $Re \in [150, 30000]$, three instability modes are excited: one, an axisymmetric pulsation of the recirculating zone with no vortex shedding; two, an axisymmetric vortex shedding associated with the shear at the periphery of the recirculating zone; and three, a spiral mode with azimuthal wavenumber 1, related to a rotation of the separation line. These instability modes are associated with four regimes which are functions of Reynolds numbers. In the range $Re \in [24, 200]$, the recirculating zone exists in an axisymmetric and steady fashion. The lower Re limit has been determined from Taneda's (1956) work. This regime has been fully described in Nakamura (1976). When $Re \in [200, 400]$,

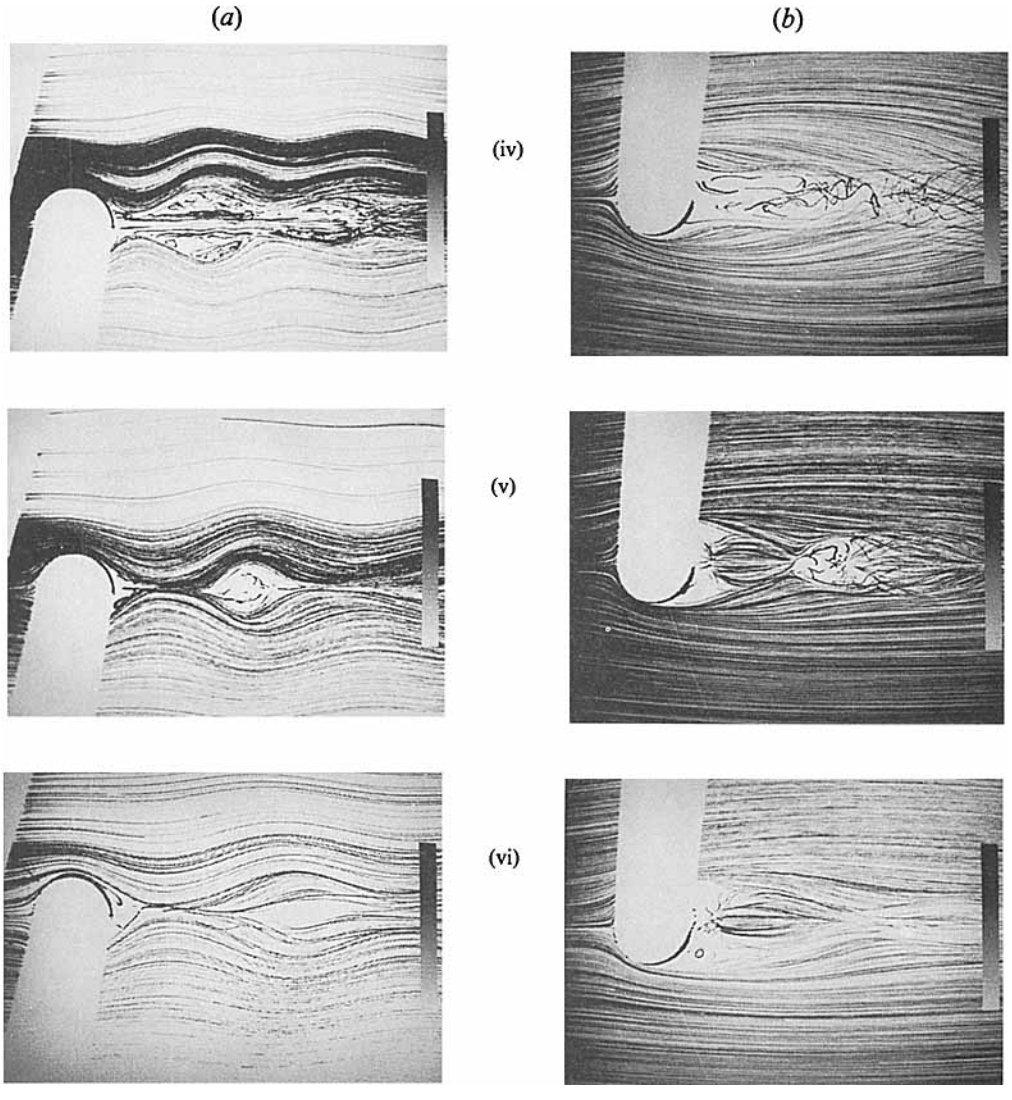

FIGURE 4 (iv–vi). For caption see facing page.

the first instability is excited and an axisymmetric pulsation of the recirculating zone with no vortex shedding is observed. In the range $Re \in [400, 800]$, the recirculating zone ceases to be axisymmetric and vortex shedding occurs. Vortex loops connected by a spiral are emitted regularly behind the sphere (figure 2*a*) and the axisymmetric vortex shedding is locked with the spiral mode. For $Re > 800$ and up to the highest value explored, $Re = 30000$, the two modes are simultaneously present but are unlocked (figure 2*b*).

The coherence of each mode is still an open question. For smaller Reynolds number ($Re \in [800, 4000]$) the spiral mode was visible on video recordings but the power spectrum exhibited no clear peak. Other careful measurements would be of interest to clarify the change from a noise-driven instability to a coherent global mode because this could confirm a transition from a convective to an absolute spiral instability. For high enough Reynolds number ($Re > 4000$) the low-frequency mode seems to be

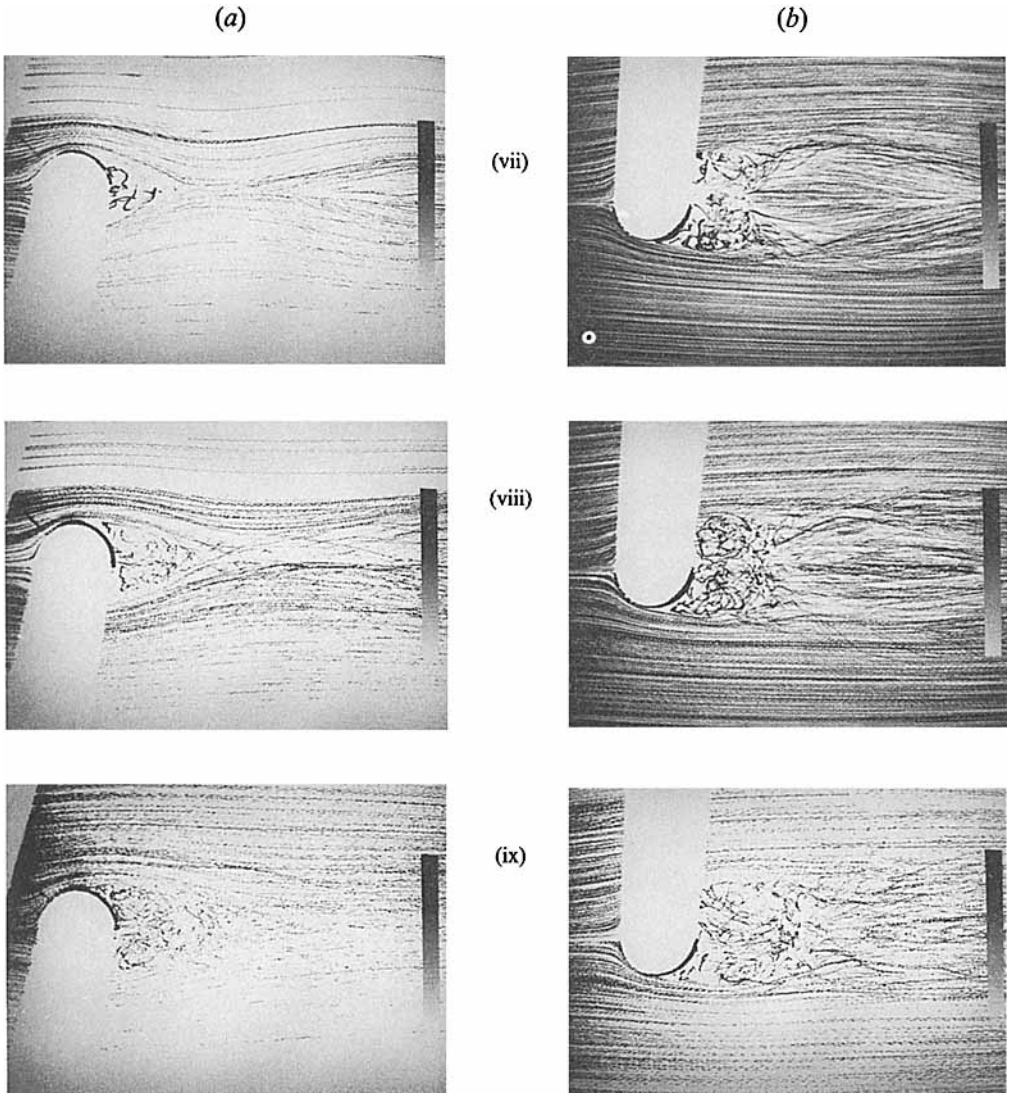

FIGURE 4. Particle streak trajectories in (*a*) the vertical central plane, and (*b*) the horizontal central plane, for $Re(1) = 2177$. (i) $F = 0.4$; (ii) $F = 0.5$; (iii) $F = 0.6$; (iv) $F = 0.7$; (v) $F = 0.9$; (vi) $F = 1.0$; (vii) $F = 1.5$; (viii) $F = 2.0$; (ix) $F = 10/\pi$.

coherent and is associated with a regular spiral as demonstrated by flow visualization and by spectral analysis of a single velocity probe carried in the wake with the sphere. This may correspond to a global resonance, where the spiral mode becomes regular with an amplitude large compared to the noise even at the sphere (Monkewitz 1988; Chomaz, Huerre & Redekopp 1988).

The Strouhal number is plotted on figure 3. The large symbols refer to the low-frequency spiral mode obtained from flow visualization by measuring the wavelength λ ($S_\lambda = 2R/\lambda$), and the Strouhal number of the Kelvin–Helmholtz instability, obtained by visual measurements of the vortex shedding frequency f' ($S' = f'(2R)/U$). The small symbols refer to probe measurements of frequency f ($S = f(2R)/U$). It is seen in figure 3 that for $Re < 800$ the two frequencies are locked and split smoothly at $Re = 800$. The

Strouhal number of the spiral mode stays nearly constant at 0.175 and the Strouhal number of the Kelvin–Helmholtz mode keeps rising with Re. The solid line, in the range $Re \in [800, 20000]$, corresponds to measurements of the Kelvin–Helmholtz wavelength λ', determined from fluorescent dye photographs. S'_λ ($S'_\lambda = R/\lambda'$) is found to follow an $Re^{\frac{1}{2}}$ law which is consistent with a Kelvin–Helmholtz instability because the shear thickness varies as the boundary-layer thickness on the sphere, proportional to $Re^{\frac{1}{2}}$.

3.2. *Stratification effects on the wake structure*

Four different wake regimes may be distinguished, depending on Froude number and also weakly on Reynolds number. As the Froude number increases from $F < 1$ to $F > 1$, there is a change from a quasi-two-dimensional (2D) wake, bounded by lee waves, to a 'saturated' lee wave (SLW) regime at $F \approx 1$ ($F \in [0.8, 1.5]$). After a transition regime (T) at $F > 1.5$, the three-dimensional (3D) homogeneous near-wake regime is recovered at $F > 4.5$. These regimes are illustrated in figure 4 by particle streak visualizations for $Re(1) = 2177$ and in figure 6 by fluorescent dye visualizations for $Re(1) = 329$ and are discussed in more detail below. The Reynolds numbers covered in the experiments thus range from 870 to 6933 in figure 4 and from 164 to 1047 in figure 6 and in some experiments with stratification the Reynolds number was as large as 50000. As will be seen from the results, the change in flow structure with Froude number is only weakly affected by Reynolds number when $F < 0.7$ and $Re > 100$. At larger values of F the flow separation angles depend more strongly on Re, and when $F > 4.5$ the near wake depends on Re as does the wake in homogeneous fluid.

3.2.1. *The quasi-two-dimensional regime*: $F \in [0.25, 0.8]$

The flow is split into three layers (figures 4(*a*)(i) and 5). In the central layer, the flow is observed to go around the sphere and the wake consists of quasi-two-dimensional, vertically coherent, motions. This quasi-two-dimensional layer is bounded above and below by two layers where the flow, going over or under the sphere, is affected by gravity waves. This partition of the flow into three distinct and nearly independent layers causes the separation line to have a nearly rectangular shape (Chashechkin & Sysoeva 1988; Chomaz *et al.* 1992). When the Froude number is progressively increased from 0.25, the thickness of the two-dimensional layer decreases and it disappears completely at about $F \approx 0.8$. In figures 4(*a*)(i) and 4(*a*)(ii), and to some extent in 4(*a*)(iii), recirculation zones exist under the waves, which Lin *et al.* (1992) termed 'lee-wave instability', with a roller formation of positive-y vorticity located under the wave crests (mainly the first one). A baroclinic vorticity generation argument is given by Lin *et al.* for this lee wave instability. From the streamlines shown in figures 4(*a*)(i) and 4(*a*)(ii) it is difficult to support these arguments. There is no indication of the wave breaking which the terminology instability would imply. The origin of the eddy motion under the wave crests is more likely due to the local shear layer thickening under the wave crest giving rise to an adverse pressure gradient. Sysoeva & Chashechkin (1986) have discussed these rollers and attribute them to Kelvin–Helmholtz instability.

The structure of the central-layer wake shows a behaviour analogous to the cylinder wake in homogeneous fluid. For $F \in [0.25, 0.5[$, called the two-dimensional detached wake regime (2DD), vortices separate periodically on each side of the sphere similar to what is observed for a cylinder at $Re > 80$ (figures 4(*b*)(i) 5*b* and 6(*b*)(i)). The side view, figure 5(*a*), shows that the wake further away from the body is composed of V-shaped structures similar to what is observed in the far-field wake at large Froude numbers (Hopfinger *et al.* 1991). These V-shaped structures are thought to be a result of the

(*a*)

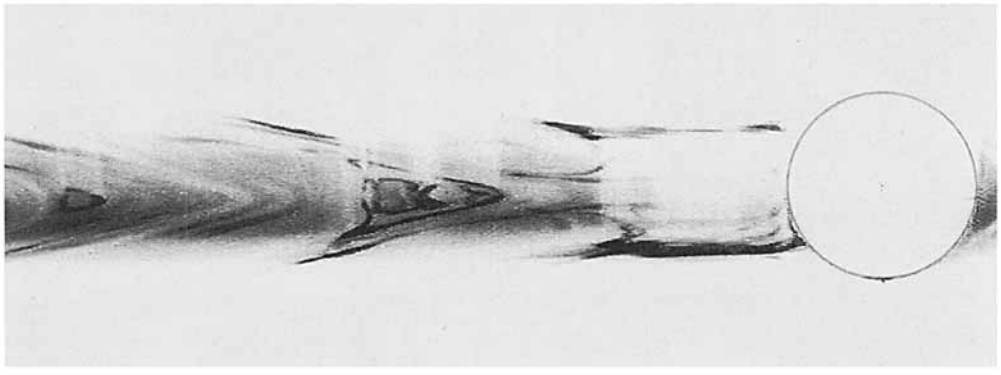

(*b*)

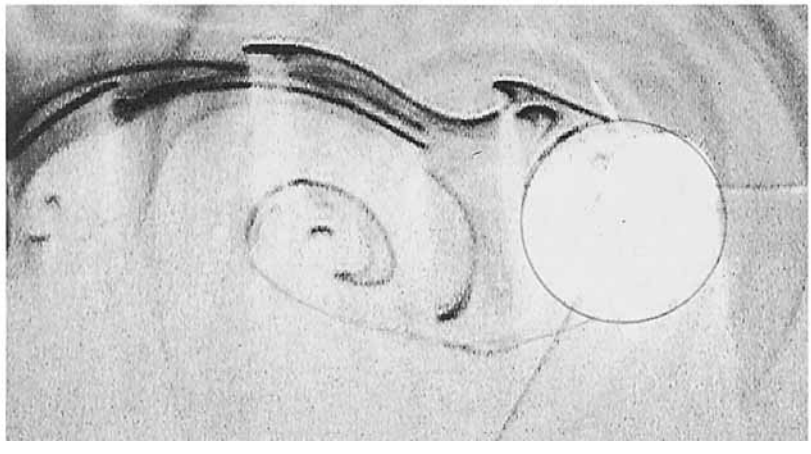

FIGURE 5. Fluorescent dye visualizations for $F = 0.3$ and $Re(1) = 1961$: (*a*) vertical central plane; (*b*) horizontal central plane.

density interfaces, which bound the two-dimensional wake above and below and which are drawn out like a string by the two-dimensional eddy structures of vertical vorticity. For $F \in [0.5, 0.7[$, which is named the two-dimensional oscillating wake regime (2DO), the two horizontal vortices do not separate but oscillate periodically, similar to the cylinder wake for $Re \in [40, 80]$ (figures 4(*b*)(iii) and 6(*b*)(ii)). For $F \in [0.7, 0.8]$, called the two-dimensional non-oscillating wake regime (2DS), the two horizontal vortices do not separate nor oscillate as for $Re \in [5, 40]$ in the cylinder case (figures 4(*b*)(iv) and 6(*b*)(iii)). Sysoeva & Chashechkin (1986) have shown that in this case the flow becomes laminar for Re smaller than 100. A plausible explanation is that the effective two-dimensional viscosity increases strongly when the thickness of the layer decreases. When $F \in [0.25, 0.7[$, the dimensionless frequency (Strouhal number) of the wake instability is close to 0.2, in agreement with the results of Lin *et al.* (1992). Brighton (1978) found experimentally that the wake behind a hemisphere in a stratified flow becomes unsteady for F smaller than 0.15, with a dimensionless shedding frequency equal to 0.44. This disagreement with our experiments is certainly related to the stress

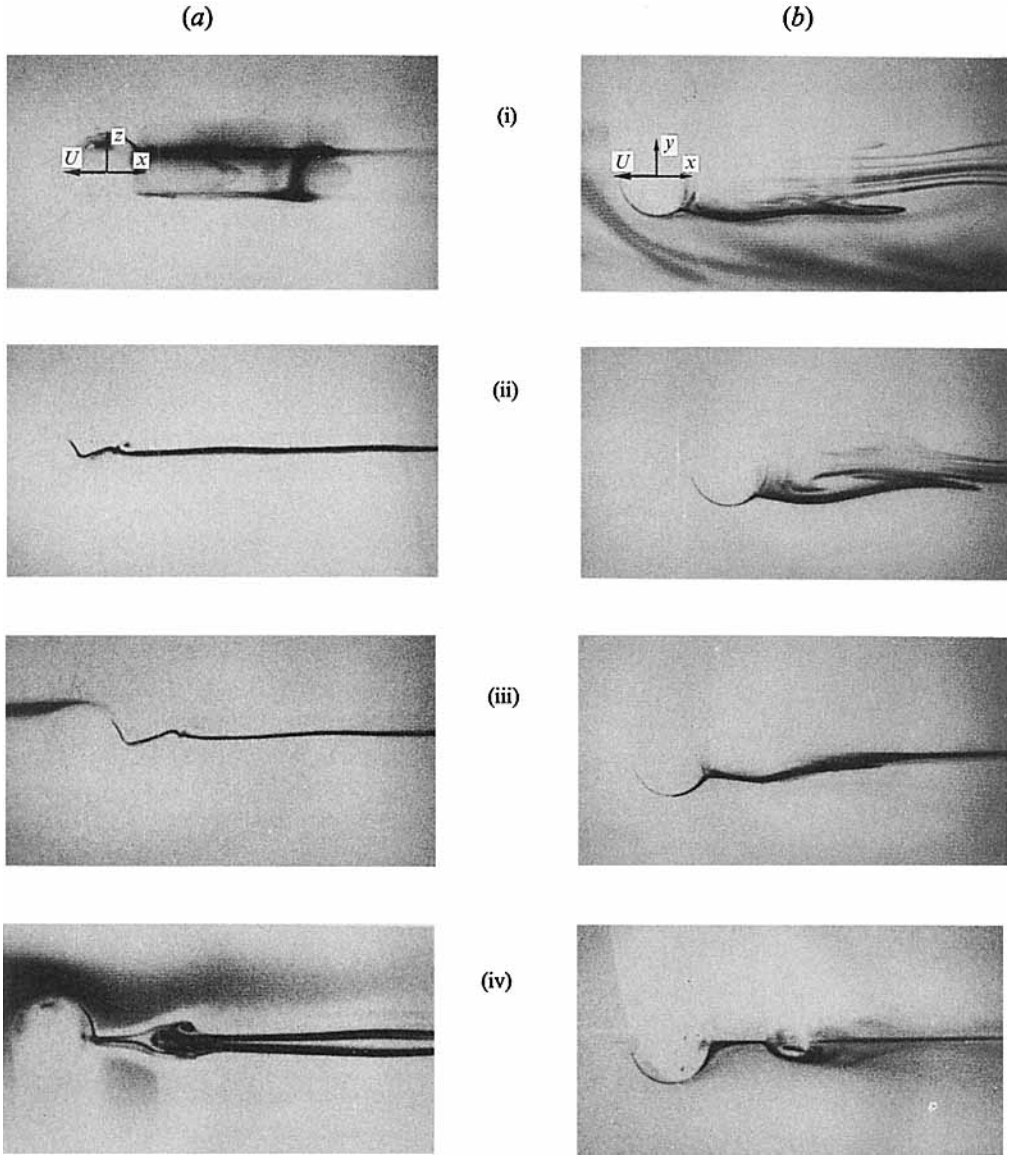

FIGURE 6 (i–iv). For caption see facing page.

exerted on the recirculating zone by the bottom of the tank, which inhibits the wake instability. More surprising is that Hanazaki (1988) did not observe this instability in his numerical simulations.

3.2.2. *The SLW regimes* $F \in [0.8, 1.5]$

This regime is dominated by a very strong lee wave of maximum amplitude $\zeta_0 = \frac{1}{2}R$. The separation is nearly suppressed throughout this region because of the depression due to the lee waves. At low Reynolds numbers (of order 100) the flow is observed to detach only at $\theta = 180°$ (θ is measured from the stagnation point), whereas at higher Reynolds numbers (> 1000), a separated flow persists owing to the competition

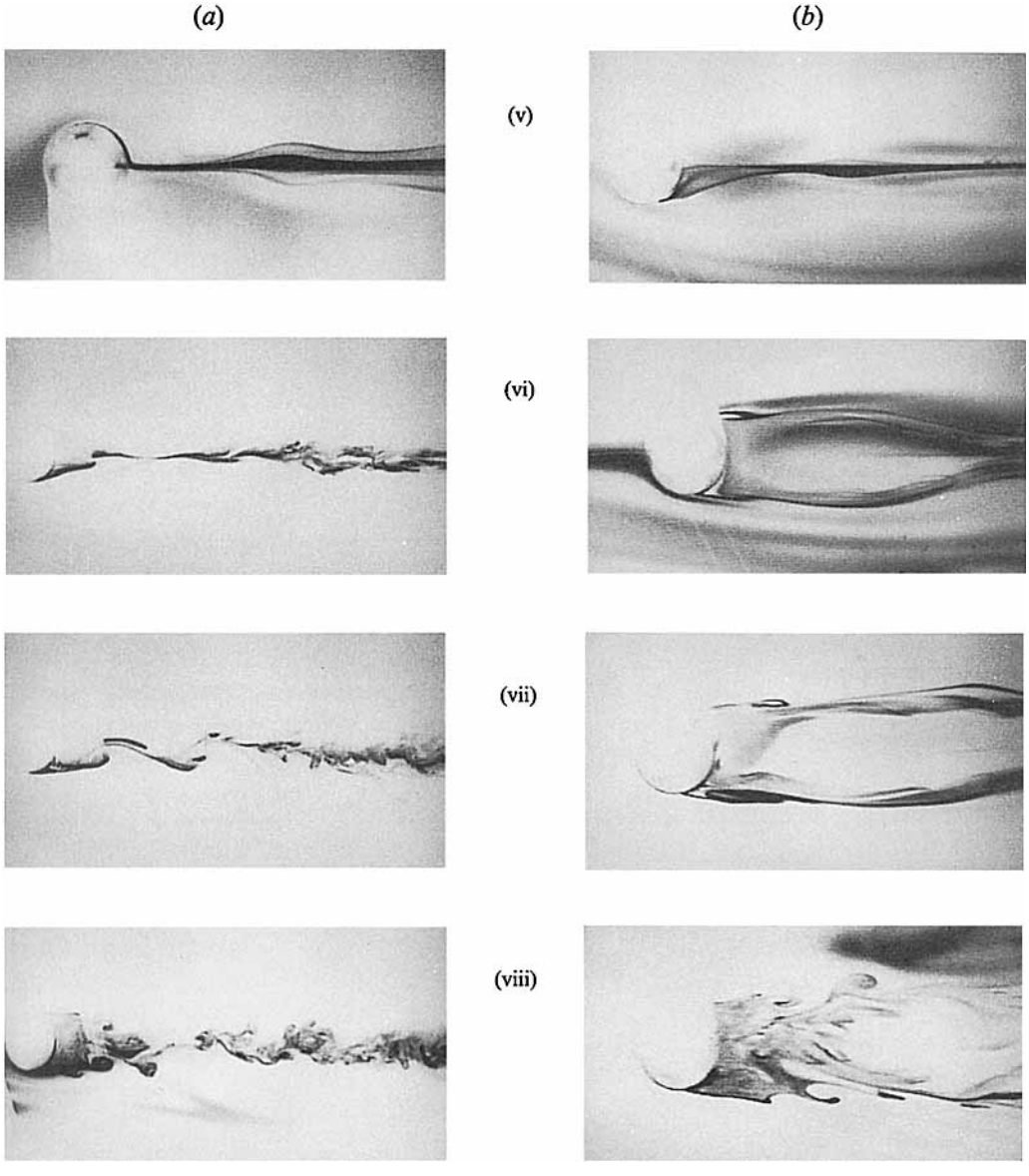

FIGURE 6. Fluorescent dye visualizations in (*a*) the vertical central plane, and (*b*) the horizontal central plane, for $Re(1) = 329$. (i) $F = 0.5$; (ii) $F = 0.6$; (iii) $F = 0.7$; (iv) $F = 0.9$; (v) $F = 1.0$; (vi) $F = 1.5$; (vii) $F = 2.0$; (viii) $F = 10/\pi$.

between turbulent pressure and lee wave pressure. We observe in figure 7 that the separation angles in the vertical and horizontal median planes evolve differently. This results in curious shapes of the separation line (see Chomaz *et al.* 1992). In the range $F \in [0.8, 0.9]$, which we call resonance conditions, the separation line has a bow-tie shape. Its size increases with Re and is reduced to a single point at small Re. A small recirculating region separated from the sphere and of uniform density is visible in figures 4(*a*)(v), *b*(v) and 6(*a*)(iv), (*b*)(iv). The topologies of the surface stress patterns related to the non-axisymmetric flow separation lines have been discussed by Lin *et al.* (1992).

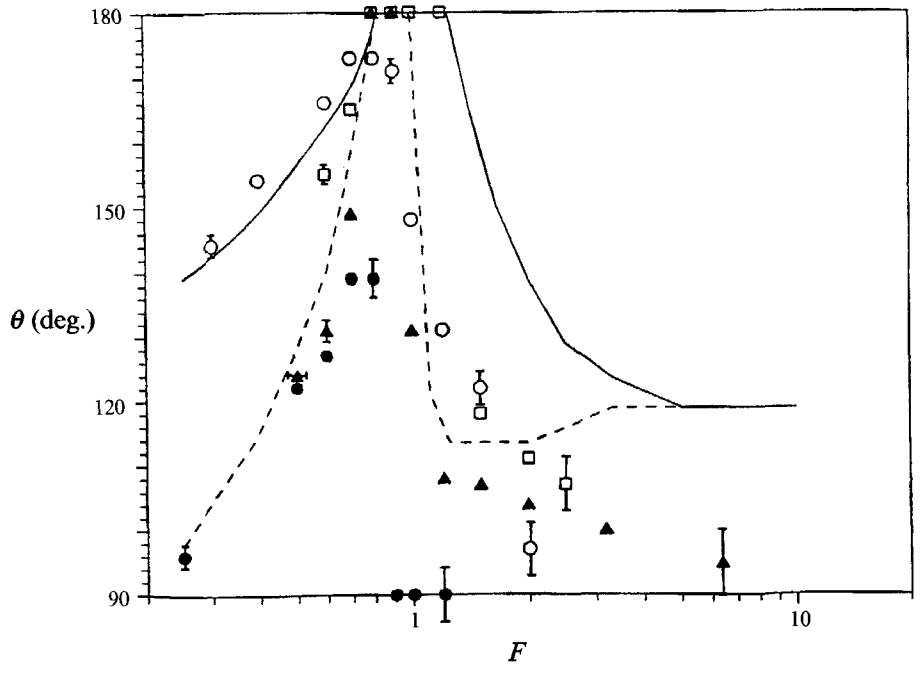

FIGURE 7. Variation with F of the separation points on the sphere in the vertical plane (open symbols) and in the horizontal plane (solid symbols). □, ▲, $Re(1) = 324$; ○, ●, $Re(1) = 1961$. ——, Hanazaki's (1988) numerical simulations in the vertical plane, – – –, in the horizontal plane.

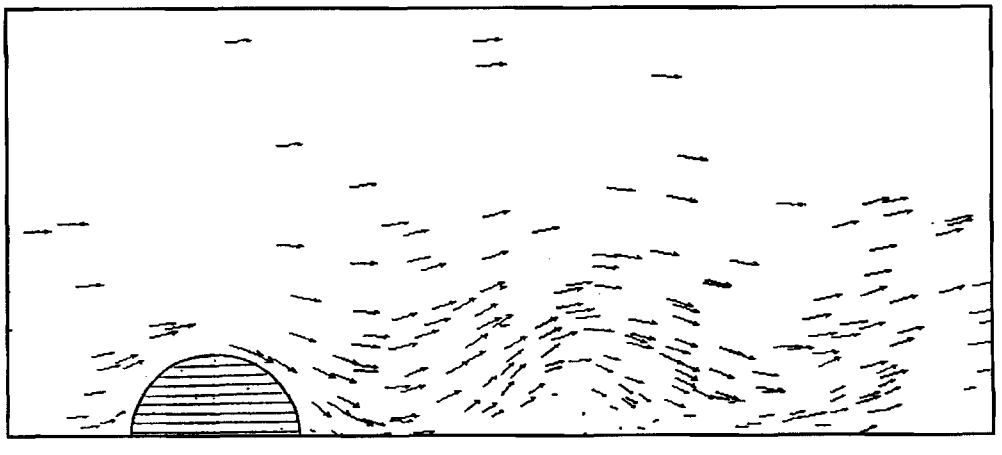

FIGURE 8. Velocity vectors relative to the sphere in the vertical central plane for $F = 0.9$ and $Re(1) = 2177$.

This resonance regime shows interesting features as demonstrated by the velocity field relative to the sphere (figure 8), calculated from particle displacements. It is seen that behind the sphere particles have a downslope velocity greater than the mean stream. In the atmosphere severe downslope winds can therefore be generated without lee wave breaking. Except close to the sphere and close to the isolated recirculation bubbles (see figures 6(*a*)(iv), (*b*)(iv)), the flow in the fluid frame corresponds only to lee wave propagation, with upward and downward motions (figure 8). The isolated

(*a*)

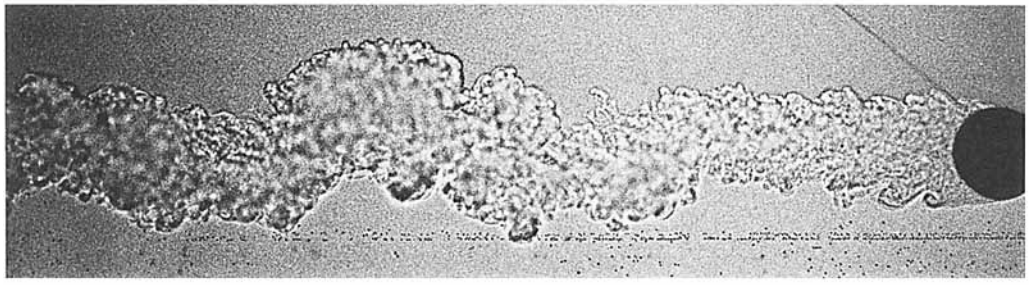

(*b*)

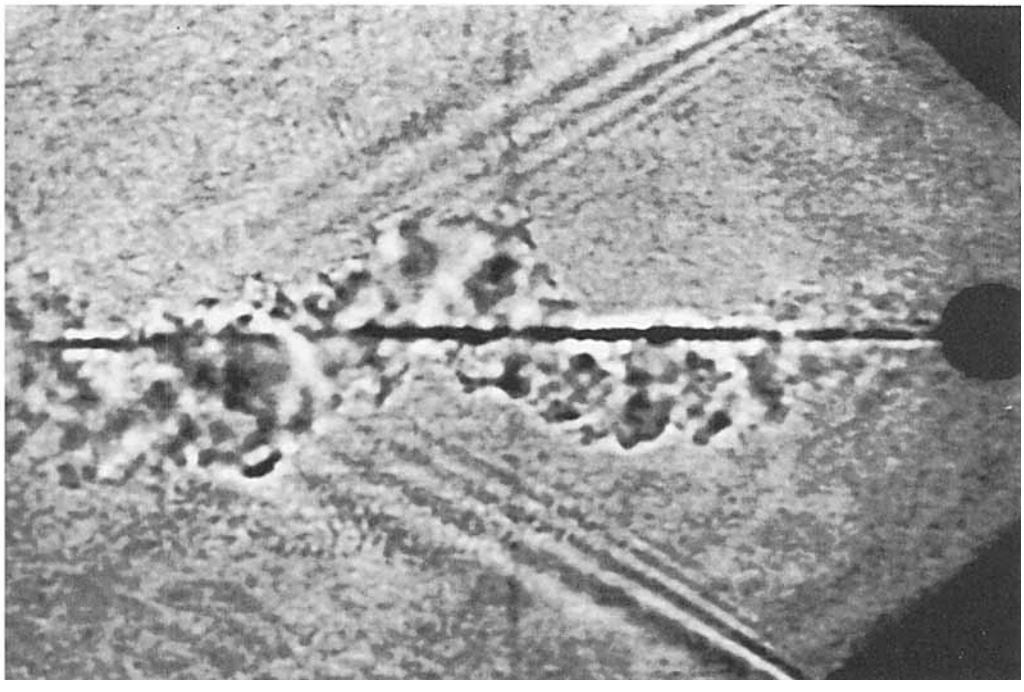

FIGURE 9. Shadowgraph visualizations of the wake for $F > 4.5$ ($Re(1) = 1354$): (*a*) side view, $F = 20/\pi$; (*b*) top view, $F = 30/\pi$ (waves on the free surface of the tank perturb the visualization from above).

circulation bubbles are steady, contrary to what is observed behind cylinders where these bubbles seem to oscillate (Boyer *et al.* 1989).

Increasing the Froude number slightly above $F = 0.9$ makes the horizontal separation angle abruptly decreases (figure 7), whereas the vertical one stays maximum or very close to the maximum. This gives a butterfly-shape or a bow-tie-shaped separation line on the sphere with a pinch in the middle. The isolated recirculating region has disappeared (figures 4(*a*)(vi) and 6(*a*)(v)) and the separation bubble is also pinched by the lee wave, and is symmetric only with respect to the vertical and horizontal median planes (see figure 6(*a*)(v), (*b*)(v)). The pinch disappears slowly when the Froude number is increased further and an elliptic separation line is recovered for

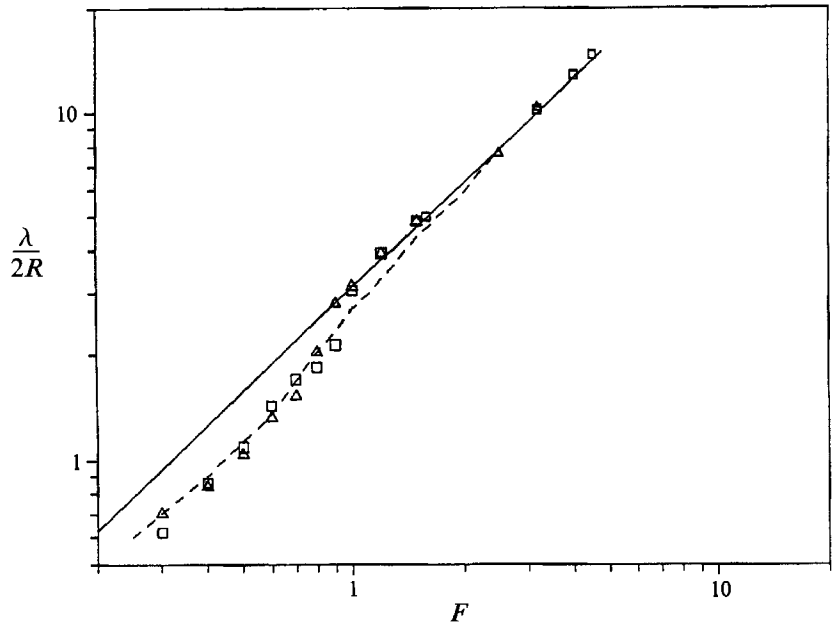

FIGURE 10. Wavelengths non-dimensionalized by $2R$ as a function of Froude number: □, $Re(1) = 2177$; △, $Re(1) = 4514$; ——, $\lambda/2R = \pi F$; – – –, Hanazaki's (1988) numerical simulations.

$F = 1.5$. The Reynolds number only weakly affects this scenario though the actual values of the separation angles do depend strongly on Reynolds number when $F > 0.7$.

3.2.3. *The T regime* $F \in [1.5, 4.5]$

This regime marks the transition between the wake dominated by the lee wave and a wake unaffected by stratification in the near field. The details of this transition are more sensitive to Reynolds number in the sense that the neutral wake structure itself is sensitive to Re. The lee wave amplitude is observed to decrease slowly as F increases (see figure 4) and the recirculating zone behind the sphere grows. For F up to 2.5, this zone is pinched in the middle by the lee wave minimum but the separation line is already a circle.

The two instability modes described in § 3.1 become excited at different F-values. The Kelvin–Helmholtz instability, which has a Strouhal number varying as $Re^{\frac{1}{2}}$ for the neutral wake, manifests itself first at a Froude number F_c, decreasing as the Reynolds number increases ($F_c = 3$ for $Re(1) = 329$ and $F_c = 1.5$ for $Re(1) = 4067$). The recirculating zone becomes unsteady for $F > 1.5$ and for $Re > 400$. Figures 6(*a*)(vi), (*a*)(vii) and (*a*)(viii) show that the mode exited does not correspond to the spiral but to a vertical oscillation. The appearance of the stable spiral instability defines the end of this regime.

3.2.4. *The 3D regime* $F > 4.5$

In this regime, the stratification has no effect on the close wake (for $Nt < 3$), so that the observed flow structure follows the one described for the neutral wake. In particular, for Re larger than 800 the regular spiral instability occurs and develops (see figures 9*a*, *b*) until it collapses under the buoyancy effect. The lee wave amplitude is small in this regime and the wavelength long compared with the length of the spiral

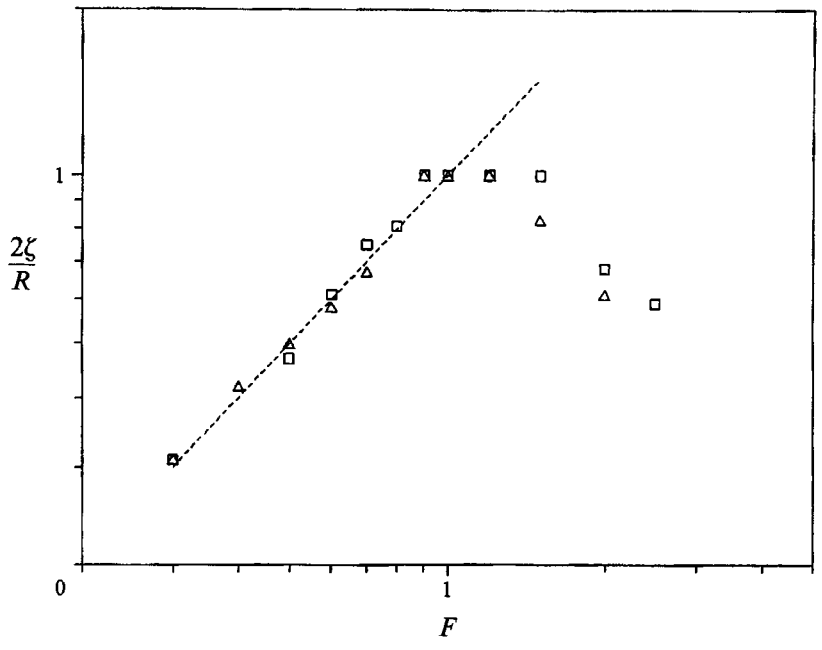

FIGURE 11. Wave amplitudes non-dimensionalized by $\frac{1}{2}R$ as a function of Froude number. □, $Re(1) = 2177$; △, $Re(1) = 4514$; ----, Sheppard's (1956) theory.

mode. Gravity waves comes essentially from the formation and collapse of the coherent spiralling wake (Chomaz *et al.* 1991).

3.3. *Lee waves and their relation to the wake structure*

In this section we present quantitative results for the lee waves, obtained from particle streak experiments. In figure 10, the wavelength measured between the first two crests of the lee wave, along the isopycnal line initially tangent to the sphere, is plotted as a function of F. Two sets of experiments have been carried out with $Re(1) = 2177$ and 4514. The measured wavelengths are in good agreement with Hanazaki's (1988) numerical results corresponding to $Re = 200$. This agreement shows that the lee wave wavelength is not dependent on the Reynolds number. Linear theory is well verified for $F > 1$, but for $F < 1$ it overestimates the wavelength. This is because the phase lines are distorted by the velocity shear at the upper and lower edges of the wake, pointed out already by Chashechkin (1989).

The wave amplitude shown in figure 11 is also independent of the Reynolds number. It is seen that in the range $F \in [0.3, 0.8]$, the amplitude increases linearly with F. In that case the amplitude of the lee wave is governed by Sheppard's argument (Snyder *et al.* 1985): a fluid particle upstream of the sphere will go over or around the sphere depending on whether its kinetic energy is larger or smaller than the potential energy necessary to pass over the sphere. This gives the relation

$$2\zeta_0/R = F$$

which is well verified by our experiments (figure 11). The amplitude variation shows a plateau around $F \in]0.9, 1.5[$. As mentioned before, this regime is dominated by a very strong lee wave having the maximum possible amplitude $\zeta_0 = \frac{1}{2}R$. It is of interest to relate the wave amplitudes with the drag measured by Lofquist & Purtell (1984). The

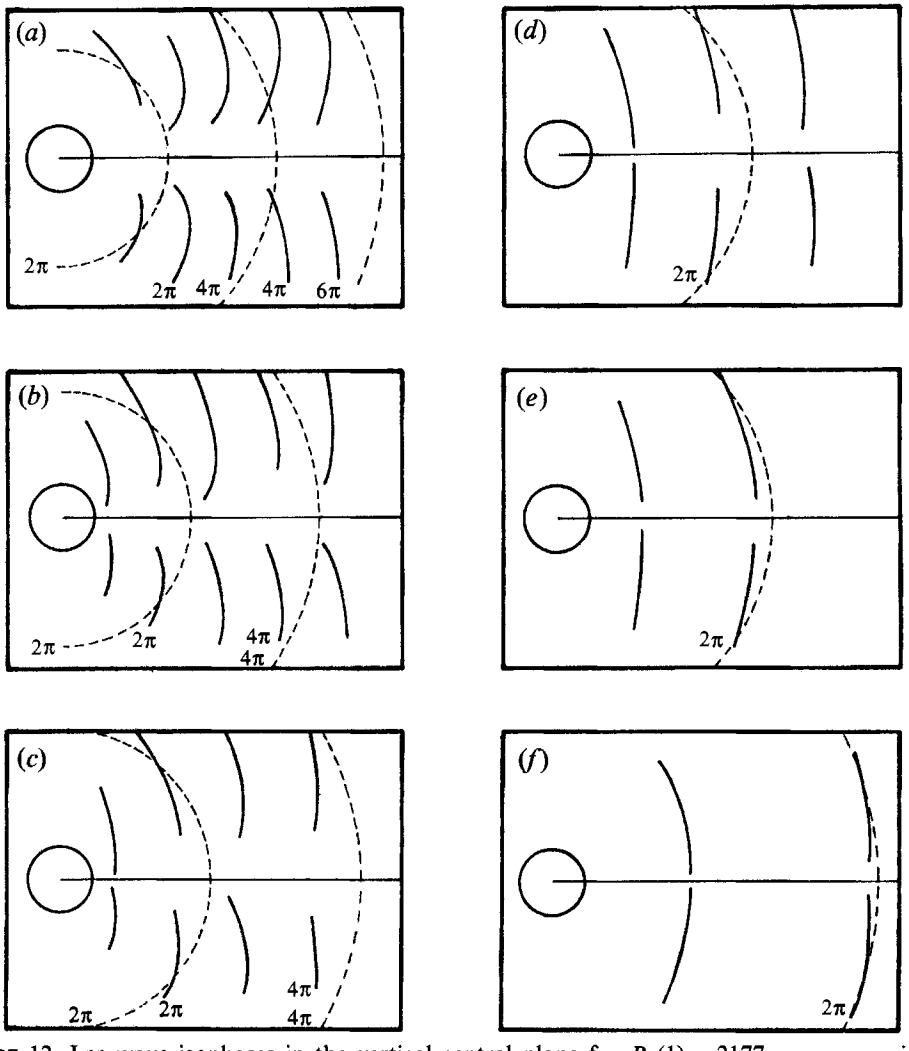

FIGURE 12. Lee wave isophases in the vertical central plane for $Re(1) = 2177$. ——, experiments (every π); – – –, linear theory (every 2π). (*a*) $F = 0.5$; (*b*) $F = 0.6$; (*c*) $F = 0.7$; (*d*) $F = 0.9$; (*e*) $F = 1.0$; (*f*) $F = 1.5$.

maximum in the lee wave drag corresponds to the maximum in wave amplitude at $F \approx 1$. Their drag curve exhibits a second peak of lesser amplitude at a value of $F \approx 0.7$ which can be explained by the appearance of the two-dimensional wake structure when $F < 0.8$, which adds to the drag. For $F < 0.7$ the drag decreases because the wave amplitude decreases. For F greater than 1.5, the lee wave amplitude decreases with F. In that case, the nonlinear interactions with the sphere become negligible and the lee wave amplitude follows approximately a $1/F$ law as predicted by linear theory (see Miles 1971 or Voisin 1991).

The lee wave patterns, in the vertical central plane, are traced by dashed lines in figure 12. We note that for small Froude numbers the isophases are less curved than those predicted by linear theory. The discrepancy is stronger close to the wake axis. This phenomenon can also be observed in the side views of the isopycnal lines numerically simulated by Hanazaki at low Reynolds number. This deviation of the lee wave pattern from theory is due to finite size of the sphere and to interactions between

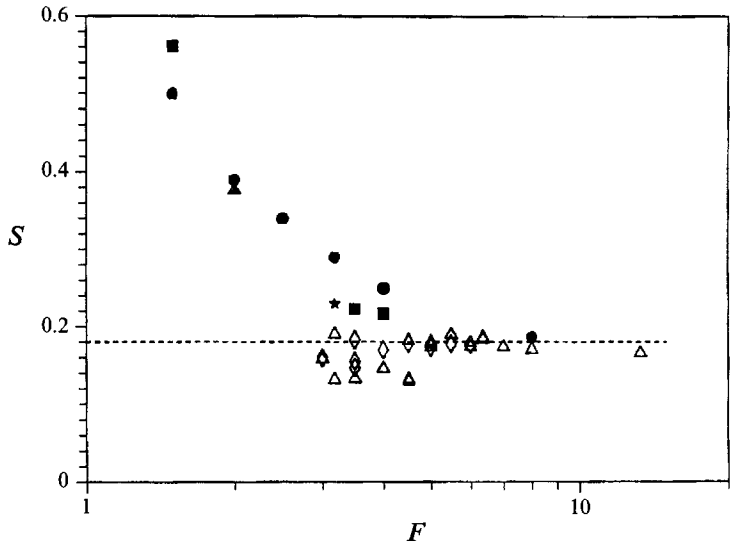

FIGURE 13. Strouhal number of low-frequency instabilities of the wake as a function of the Froude number measured from spectral analysis of probe signals (open symbols) and vertical fluorescein dye visualizations (filled symbols): △, $Re(1) = 2614$ ($R = 3.6$ cm); ◇, $Re(1) = 2641$ ($R = 3.6$ cm); ●, $Re(1) = 722$ ($R = 1.12$ cm); ■, $Re(1) = 1961$ ($R = 2.5$ cm); ▲, $Re(1) = 4246$ ($R = 3.6$ cm); ★, $Re(1) = 324$ ($R = 1.12$ cm).

the lee wave and the wake, which decreases as F increases. Figure 12(f) shows that for $F \geqslant 1.5$ the lee wave phase lines are closely approximated by linear theory.

3.4. *Characteristic frequency of the wake*

The Strouhal number of the wake instabilities is plotted on figure 13 as a function of F. In the large tank, for $U < 10$ cm s^{-1} (small F), the towing carriage slightly vibrates and for this reason the characteristic frequency for $F \in [1.5, 4[$ were determined from visualizations of the type shown in figure 6, performed in the small tank. These measurements are shown by filled symbols in figure 13. The Strouhal number for $F \geqslant 3$ was obtained from the spectral analysis of conductivity and hot-films probe signals. It is noted in figure 13 that for $F \geqslant 4.5$, the near wake is unaffected by stratification and the spiral mode appears with a fixed Strouhal number of 0.175. Figure 14 presents a comparison between the power spectra of the vertical velocity measured at $x = 2R$ and $z = R$ in the turbulent neutral wake ($F = \infty$) and in the stratified wake with $F = 4.5$. In both cases, we observe a frequency peak corresponding to a Strouhal number $S = 0.175$. The conductivity probe mounted on the sphere surface, which measures the time variation of the detachment point, gives the same value of S. At the higher frequencies the spectrum follows roughly a $k^{-\frac{5}{3}}$ law, characterizing three-dimensional turbulence. When the stratification effects increase, the wake instability loses its axial symmetry. We have already noticed on figure 6 that for $F \in [1.5, 4.5]$, the instability does not correspond to a spiral mode but to a vertical oscillation with corresponding Strouhal number greater than 0.17. It is seen in figure 13 that the value of the Strouhal number of this oscillating mode increases as F decreases until $F \approx 1.5$. For $F < 1.5$, the recirculating zone is forced by a strong lee wave which prevents it from becoming unsteady.

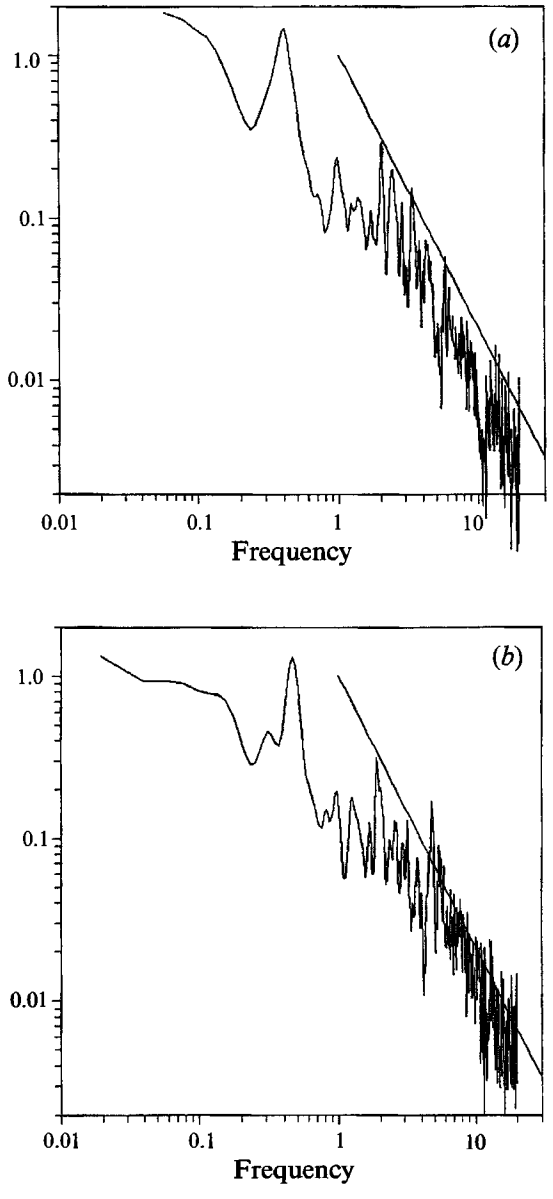

FIGURE 14. Spectrum of the vertical velocity measured at the location $z = R$ and $x = 2R$, for $Re = 11765$. (*a*) $F = \infty$; (*b*) $F = 4.5$.

4. Conclusions and further discussion

For the homogeneous wake the results of Kim & Durbin are confirmed, and the instability modes have been more clearly identified by means of flow visualizations. The Kelvin–Helmholtz instability on the periphery of the recirculating zone gives rise to the shedding of vortex rings coherently or partially coherently along the perimeter. The spiral instability is related to a rotation of the recirculation zone and consequently of the separation line. The wake is stable up to $Re = 200$, then a low-frequency symmetric pulsation occurs up to $Re = 400$ with no vortex shedding. From 400 to 800, the Kelvin–Helmholtz and the spiral mode are locked together. At $Re = 800$, the two

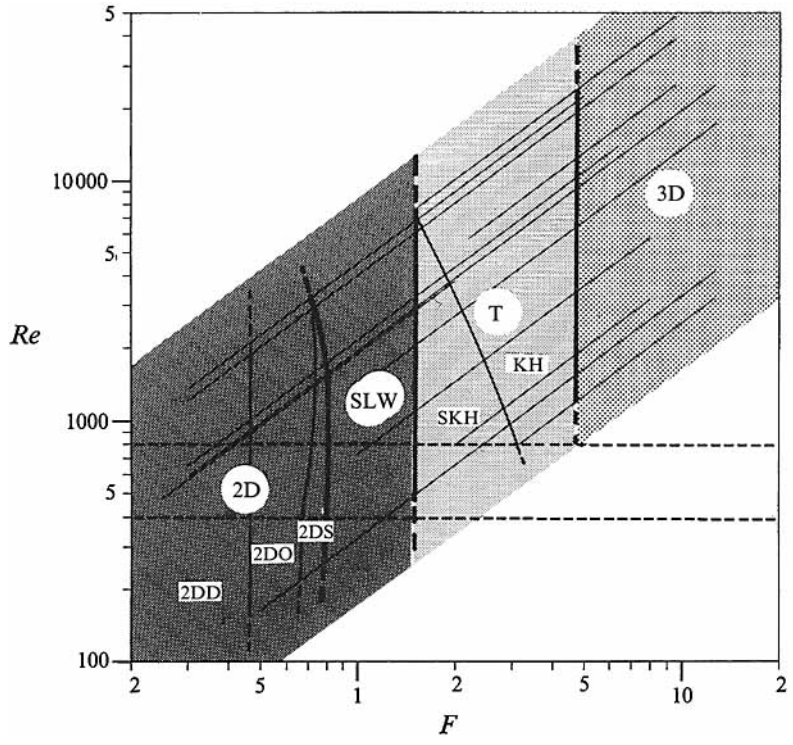

FIGURE 15. Flow regime diagram (F, Re): 2D, two-dimensional wake regime (2DD, two-dimensional detached wake; 2DO, two-dimensional oscillating wake, 2DS, two-dimensional non-oscillating wake); SLW, 'saturated' lee wave regime; T, transition regime (SKH, without Kelvin–Helmholtz instability; KH, with Kelvin–Helmholtz instability); 3D, three-dimensional wake regime. Horizontal dashed lines are drawn at $Re = 400$ and 800 to recall the transitions in the homogeneous wake. Each thin line indicates a set of experiments at fixed $Re(1)$. Each data set contains between 12 and 24 values of F.

modes become unlocked; the Strouhal number of the Kelvin–Helmholtz instability continues to grow as $Re^{\frac{1}{2}}$, and the spiral instability is irregular and weak with a Strouhal number close to 0.2. Around $Re = 4000$ the spiral mode picks up and takes a fixed Strouhal number value of 0.175, at least up to the limit of our investigation of $Re = 30000$. This strengthening of the regular spiral mode is consistent with global instability behaviour (Monkewitz 1988).

The addition of buoyancy forces breaks the axial symmetry and radically modifies the picture. We define four general flow regimes based on the Froude number and depending only weakly on Reynolds number. When $F < 0.8$, a median horizontal layer downstream of the sphere consists of a quasi-two-dimensional wake, similar to cylinder wake, bounded above and below by two lee-wave layers. When $F \in [0.8, 1.5]$, the lee wave saturates at the value $\zeta_0 = \frac{1}{2}R$ and almost no separation occurs, making the flow totally governed by the lee waves. The range $F \in [1.5, 4.5]$ marks the transition regime where the lee wave amplitude diminishes and progressively liberates the wake flow: first the Kelvin–Helmholtz instability and then the spiral instability appear. Finally, the homogeneous wake regime is recovered, in the near field, for $F > 4.5$. At these large Froude numbers the lee wave amplitude is negligible and the flow outside the wake is dominated by random waves emitted by the turbulent wake collapse. The downstream evolution of wake itself can be characterized by the non-dimensional time Nt

(Hopfinger *et al.* 1991). The spiral structure persists up to $Nt \approx 2.5$ to 3 and any vertical overturning ceases when $Nt \approx 15$. The far-field collapsed wake begins at about $Nt \approx 20$.

The present results overlap to some extent the results presented in the paper by Lin *et al.* (1992) which emphasizes the small Froude and Reynolds number regimes. Their results concerning the low Froude number two-dimensional wake structure and the deviation of the lee-wave wavelength from linear theory are practically the same as ours. Their paper contributes very little to the large Froude number ($F > 1.5$) wake structure, however. In order to understand this regime, it is essential to study the homogeneous wake as well. An attempt was made in this direction by Lin *et al.* but the results are too sketchy to be of any use; the spiral mode for instance is completely ignored (see their figure 26). This flawed some of this conclusions concerning the different transitions in their paper. For this reason the transition T, with Kelvin–Helmholtz instability (KH) and without (SKH), in the regime diagram shown in figure 15, could not be identified by Lin *et al.* The saturated lee wave (SLW) regime in figure 15 corresponds partially to their N & S regimes. We also cannot agree with the wave instability interpretation of the recirculating zones under the lee waves at $0.3 < F < 0.8$. The origin of these eddies is more likely a consequence of the shear-layer thickening under the wave crest, giving rise to an adverse pressure. Sysoeva & Chashechkin (1986) on the other hand attribute it to Kelvin–Helmholtz instability.

Further differences exist in the relationship between the Strouhal number and F, in the interpretation of the wave drag and in the dependence of the separation angles on Reynolds number, discussed in Chomaz *et al.* (1992). Considering the complexity of the wake structure of spheres, in particular with stratification, the results presented in the present paper are of importance to the understanding of stratified wakes.

This work was supported by Météo-France and contract DRET number 90-233. It was made possible by the team SPEA of the French Met Office and we wish to thank for their kind help, enthusiasm and efficiency: B. Beaudoin, J. C. Boulay, A. Butet, C. Niclot, M. Perrier, S. Lassus-Pigat and H. Schaffner.

REFERENCES

ACHENBACH, E. 1974 Vortex shedding from spheres. *J. Fluid Mech.* **62**, 209–221.

BONNETON, P. & CHOMAZ, J. M. 1992 Instabilities of the wake generated by a sphere. *C. R. Acad. Sci. Paris* **314**, (II), 1001–1006.

BOYER, D. L., DAVIES, P. A., FERNANDO, H. J. S. & ZHANG, X. 1989 Linearly stratified flow past a horizontal circular cylinder. *Phil. Trans. R. Soc. Lond.* A **328**, 501–528.

BRIGHTON, P. W. M. 1978 Strongly stratified flow past three-dimensional obstacles. *Q. J. R. Met. Soc.* **104**, 289–307.

CHASHECHKIN, Y. D. 1989 Hydrodynamics of a sphere in a stratified fluid. *Fluid Dyn.* **24**, 1–7.

CHASHECHKIN, Y. D. & SYSOEVA, E. Y. 1988 Fine structure and symmetry of the wake past a sphere in a stratified liquid. In *Proc. 17th Session of BSHC, (Varna, Bulgaria, 1988)*, vol. 1, p. 10-1.

CHOMAZ, J. M., BONNETON, P., BUTET, A., HOPFINGER, E. J. & PERRIER, M. 1991 Gravity wave patterns in the wake of a sphere in a stratified fluid. In *Proc. Turbulence 89: Organized Structures and Turbulence in Fluid Mechanics* (ed. M. Lesieur & O. Métais), pp. 489–503. Kluwer.

CHOMAZ, J. M., BONNETON, P., BUTET, A., HOPFINGER, E. J. & PERRIER, M. 1992 Froude number dependence of the flow separation line on a sphere towed in a stratified fluid. *Phys. Fluids* **4**, 254–258.

CHOMAZ, J. M., HUERRE, P. & REDEKOPP, L. G. 1988 Bifurcations to local and global modes in spatially developing flow. *Phys. Rev. Lett.* **60**, 25–28.

DAVIES, R. E. 1969 The two-dimensional flow of a stratified fluid over an obstacle. *J. Fluid Mech.* **36**, 127–144.

HANAZAKI, H. 1988 A numerical study of three-dimensional stratified flow past a sphere. *J. Fluid Mech.* **192**, 393–419.

HOPFINGER, E. J., FLÖR, J. B., CHOMAZ, J. M. & BONNETON, P. 1991 Internal waves generated by a moving sphere and its wake in a stratified fluid. *Exps Fluids* **11**, 255–261.

HUNT, J. C. R. & SNYDER, W. H. 1980 Experiments on stably and neutrally stratified flow over a model three-dimensional hill. *J. Fluid Mech.* **96**, 671–704.

KIM, H. J. & DURBIN, P. A. 1988 Observations of the frequencies in a sphere wake and of drag increase by acoustic excitation. *Phys. Fluids* **31**, 3260–3265.

LIN, J. T. & PAO, Y. H. 1979 Wakes in stratified fluids. *Ann. Rev. Fluid Mech.* **11**, 317–338.

LIN, Q., LINDBERG, W. R., BOYER, D. L. & FERNANDO, H. J. S. 1992 Stratified flow past a sphere. *J. Fluid Mech.* **240**, 315–354.

LOFQUIST, K. E. B. & PURTELL, L. P. 1984 Drag on a sphere moving horizontally through a stratified liquid. *J. Fluid Mech.* **148**, 271–284.

LONG, R. R. 1955 Some aspects of the flow of stratified fluids. III. Continuous density gradients. *Tellus* **7**, 341–357.

MILES, J. W. 1971 Internal waves generated by a horizontally moving source. *Geophys. Fluid Dyn.* **2**, 63–87.

MILES, J. W. & HUPPERT, H. E. 1968 Lee waves in a stratified flow. Part 2. Semi-circular obstacle. *J. Fluid Mech.* **33**, 803–814.

MONKEWITZ, P. A. 1988 A note on vortex shedding from axisymmetric bluff bodies. *J. Fluid Mech.* **192**, 561–575.

NAKAMURA, I. 1976 Steady wake behind a sphere. *Phys. Fluids* **19**, 5–8.

QUENEY, P. 1948 The problem of air flow over mountains: a summary of theoretical studies. *Bull. Am. Met. Soc.* **29**, 16–26.

SHEPPARD, P. A. 1956 Airflow over mountains. *Q. J. R. Met. Soc.* **82**, 528–529.

SNYDER, W. H., THOMPSON, R. S., ESKRIDGE, R. E., LAWSON, R. E., CASTRO, I. P., LEE, J. T., HUNT, J. C. R. & OGAWA, Y. 1985 The structure of strongly stratified flow over hills: dividing-streamline concept. *J. Fluid Mech.* **152**, 249–288.

SYSOEVA, E. Y. & CHASHECHKIN, Y. D. 1986 Vortex structure of a wake behind a sphere in a stratified fluid. *J. Appl. Mech. Tech. Phys.* **27**, 190–196.

TANEDA, S. 1956 Studies on the wake vortices (III). Experimental investigation of the wake behind a sphere at low Reynolds numbers. *Res. Inst. Appl. Mech., Kyushu University, Fukuoka, Japan, Rep.* **4**, pp. 99–105.

VOISIN, B. 1991 Rayonnement des ondes internes de gravité. Application aux corps en mouvement. PhD thesis, Paris 6 University.